Journal of Engineering Physics and Thermophysics, Vol. 83, No. 2, 2010

CONJUGATE HEAT TRANSFER IN A ROTATING DISC WITH HOLES

K. N. Volkov

UDC 532.529

Problems connected with the simulation of conjugate heat transfer in the flow of a viscous compressible fluid past a rotating disc with holes are considered. The discretization of the equations describing the temperature distribution inside a solid body and the fluid flow characteristics, the construction of computational meshes, and the control of the integration time step are considered. The results of the calculations of the metal temperature at control points of the model and the heat transfer coefficient distribution over its boundaries are presented.

Keywords: *conjugate heat transfer, rotating disc, numerical simulation, turbulence.*

Introduction. A disc rotating in an unbonded viscous fluid mass is the simplest geometric configuration of the gas turbine rotor.

In the coupled thermal analysis, the results of one analysis are given as loads for the other and it plays an important part in the process of designing and optimizing many technical devices, including gas turbines, compressors, and heat-transfer systems [1–12]. Investigation of the thermal action of the fluid flow on the structure units makes it possible to determine potentially problematic points of these units and take timely measures to ensure their reliability and normal operation.

The thermal analysis consists in calculating the temperature distribution and the thermal parameters in the system. It is based on the heat balance equation obtained in accordance with the energy conservation law, for whose discretization the finite-element method (FEM) is usually used. In addition to the calculation of the temperature field, as a result of the thermal analysis, the heat flow density at the boundary of the system and the heat transfer coefficients are determined (with account for the given ambient temperature).

The turbulent flow of a viscous compressible fluid is described by Reynolds-averaged Navier–Stokes equations closed by means of a particular turbulence model, for whose discretization the finite-volume method (FVM) is usually used. As a result of the integration of the Reynolds equations, the velocity, pressure, and temperature distributions inside the region occupied by the fluid and on its boundaries are found.

To simulate the fluid flow and calculate the thermal loads in a solid body, the finite-element analysis modulus (FEA-modulus) for calculating the temperature field in a solid body and the modulus for calculating the fluid dynamics (CFD-modulus) are used. The procedure of exchanging boundary values between different models requires the realization of an adequate communication subprogram. In the case of noncoincidence of the finite-element mesh (usually with triangular cells) and the finite-volume mesh (which can be both structured and nonstructured) at the interface, interpolation of the boundary values is used. Such an approach is realized in [8–13] and is used successfully to solve applied problems of various classes.

In so doing, it is usually assumed that the restructuring time of the temperature field in the fluid is much shorter than the restructuring time of the temperature field in the solid body (the flow has time to adjust to the change in the boundary conditions). For each characteristic point or portion of the loading cycle characterized by constancy of some of the parameters (for example, angular rotational velocity of the rotor), a separate CFD-model is constructed, and calculations of the fluid flow field are carried out in a stationary formulation. It is possible, in principle, to use one CFD-model for various points of the loading cycle, but this requires additional iterations for obtaining an acceptable fluid flow field.

The features of realizing a sequential approach to the conjugate thermal simulation in the regions formed by the moving (rotor) and fixed (stator) walls are considered in [12]. Unlike the conventional approach [8–10], where be-

University of Surrey Guildford, Surrey GU2 7XH, Great Britain; email: dsci@mail.ru. Translated from Inzhenerno-Fizicheskii Zhurnal, Vol. 83, No. 2, pp. 273–283, March–April, 2010. Original article submitted May 12, 2009.

1062-0125/10/8302-0291

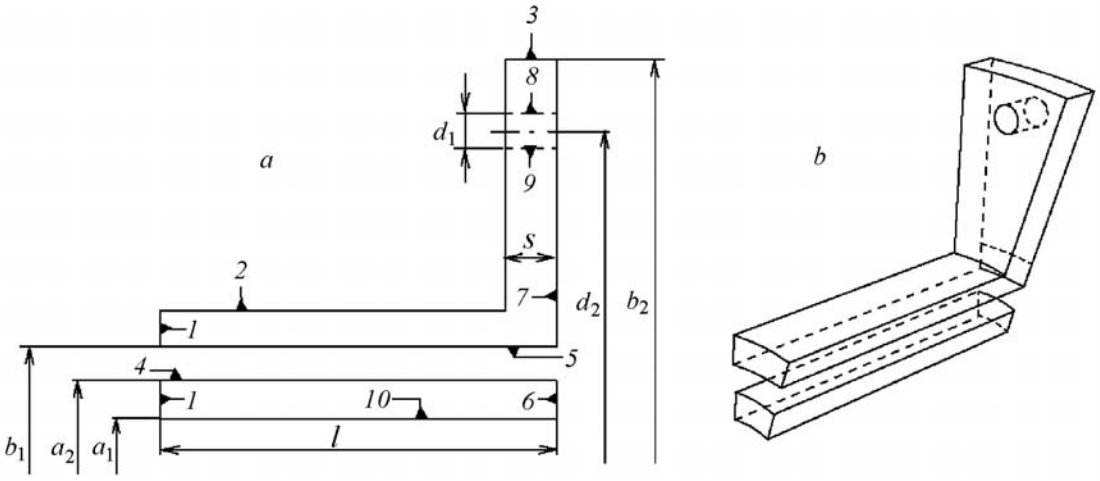

Fig. 1. Two-dimensional (a) and three-dimensional (b) geometrical models.

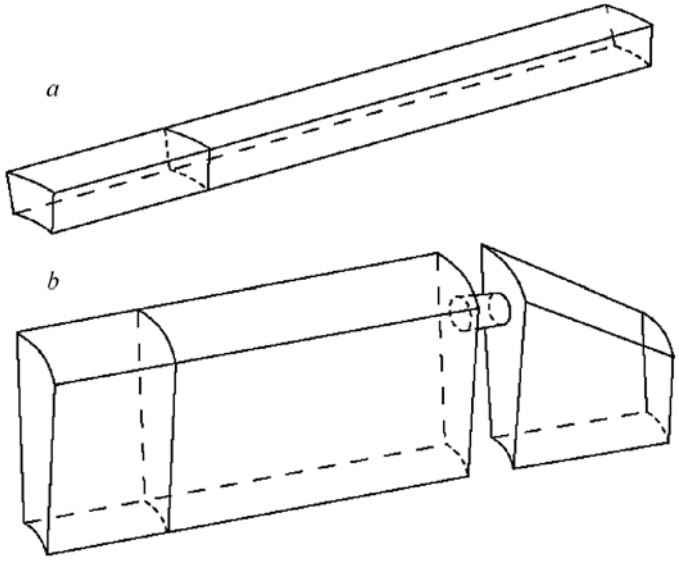

Fig. 2. Regions occupied by the fluid.

tween different computational moduli fluid and metal temperatures are transferred, in the approach of [12] the metal temperature is transferred from the FEA-modulus to the CFD-modulus, and in the opposite direction the thermal flows and the fluid temperature are transferred. Such a realization makes it possible to stabilize the numerical calculations and avoid problems connected with divergence of the iteration procedure [11–13].

The approach developed in [12, 13] is used for the coupled thermal analysis of a disc rotating in an unbounded mass of a viscous compressible fluid and having holes for fastening bolts.

Geometry of the Calculation Region. Consider a system consisting of a rotating disc having 24 holes spaced at regular intervals and a shaft.

In the calculations, an axisymmetric model (Fig. 1a) or a three-dimensional model in the form of a sector with an opening of 15^{o} (Fig. 1b) are used. The inner and outer radii of the shaft are a_1 = 0.1 m and a_2 = 0.12, and the inner and outer radii of the disc are b_1 = 0.14 m and b_2 = 0.3 m, respectively. The radius of the hole and the radial coordinate of its center are d_1 = 0.01 m and d_2 = 0.26 m, and the thickness of the disc and the length of the calculation region are s = 0.03 m and l = 0.23 m, respectively.

The three-dimensional regions occupied by the fluid are shown in Fig. 2. Region I (Fig. 2a) takes into account the fluid flow in the model gap between the rotor and the shaft, and region II (Fig. 1b) takes into account the influence of the external flow on the heat transfer of the rotating disc and the flow in the hole. For the transfer of the

boundary conditions between the finite-element and finite-volume models, to the inlet cross-section of each region an additional block of length $l/3$, where l is the length of the calculation region in the axial direction, is joined.

Basic Equations. The temperature providing the fulfillment of the condition of coincidence of the heat flows in the fluid and the solid body at the interface is determined on the basis of the iteration procedure.

In the Cartesian coordinate system, the energy balance equation has the form

$$\rho c \frac{\partial T}{\partial t} = \frac{\partial}{\partial x_i}\left(\lambda_{ij} \frac{\partial T}{\partial x_j}\right). \tag{1}$$

The internal heat sources in Eq. (1) are neglected.

For the rotor material (moving wall) titanium is used, and for the stator material (fixed wall) steel is used. The thermophysical properties are referenced with account for their temperature dependence.

The nonstationary flow of a viscous compressible fluid is described by Reynolds-averaged Navier–Stokes equations and the equations of the k–ε turbulence model, which in the Cartesian coordinate system (x, y, z) are given in the form

$$\frac{\partial \mathbf{Q}}{\partial t} + \frac{\partial \mathbf{F}_x}{\partial x} + \frac{\partial \mathbf{F}_y}{\partial y} + \frac{\partial \mathbf{F}_z}{\partial z} = \mathbf{H}. \tag{2}$$

Equation (1) is completed by the equation of state of an ideal gas

$$p = (\gamma - 1)\,\rho\left[e - \frac{1}{2}\left(v_x^2 + v_y^2 + v_z^2 - \omega^2 r^2\right)\right].$$

The vector of conservative variables and the flow vectors have the following form:

$$\mathbf{Q} = \begin{pmatrix} \rho \\ \rho v_x \\ \rho v_y \\ \rho v_z \\ \rho e \\ \rho k \\ \rho \varepsilon \end{pmatrix}, \quad \mathbf{F}_x = \begin{pmatrix} \rho v_x \\ \rho v_x v_x + p - \tau_{xx} \\ \rho v_x v_y - \tau_{xy} \\ \rho v_x v_z - \tau_{xz} \\ (\rho e + p)\, v_x - v_x \tau_{xx} - v_y \tau_{xy} - v_z \tau_{xz} + q_x \\ \rho v_x k - \alpha_x \\ \rho v_x \varepsilon - \beta_x \end{pmatrix},$$

$$\mathbf{F}_y = \begin{pmatrix} \rho v_y \\ \rho v_y v_x - \tau_{yx} \\ \rho v_y v_y + p - \tau_{yy} \\ \rho v_y v_z - \tau_{yz} \\ (\rho e + p)\, v_y - v_x \tau_{yx} - v_y \tau_{yy} - v_z \tau_{yz} + q_y \\ \rho v_y k - \alpha_y \\ \rho v_y \varepsilon - \beta_y \end{pmatrix},$$

$$\mathbf{F}_z = \begin{pmatrix} \rho v_z \\ \rho v_z v_x - \tau_{zx} \\ \rho v_z v_y - \tau_{zy} \\ \rho v_z v_z + p - \tau_{zz} \\ (\rho e + p)\, v_z - v_x \tau_{zx} - v_y \tau_{zy} - v_z \tau_{zz} + q_z \\ \rho v_z k - \alpha_z \\ \rho v_z \varepsilon - \beta_z \end{pmatrix}.$$

The noninertial character of the reference system is taken into account by introducing into the source term the Coriolis and centrifugal force

$$\mathbf{H} = \begin{pmatrix} 0 \\ 0 \\ \rho\omega\,(y\omega + 2v_z) \\ \rho\omega\,(z\omega - 2v_y) \\ 0 \\ P - \rho\varepsilon \\ c_{\varepsilon 1}\varepsilon\,(P - c_{\varepsilon 2}\rho\varepsilon)/k \end{pmatrix}.$$

The viscous stress tensor components and the heat flow tensor components are obtained from the relations

$$\tau_{ij} = \mu_e\left(\frac{\partial v_i}{\partial x_j} + \frac{\partial v_j}{\partial x_i} - \frac{2}{3}\frac{\partial v_k}{\partial x_k}\delta_{ij}\right), \quad q_i = -\lambda_e\frac{\partial T}{\partial x_i}.$$

The effective viscosity is calculated as a sum of the molecular and turbulent viscosities, and the effective heat conductivity is expressed in terms of the viscosity and the Prandtl number:

$$\mu_e = \mu + \mu_t, \quad \lambda_e = c_p\left(\frac{\mu}{\mathrm{Pr}} + \frac{\mu_t}{\mathrm{Pr}_t}\right).$$

The working medium is air (Pr = 0.72, Pr_t = 0.9). To obtain molecular viscosity values depending on the temperature, the Sutherland law is used. The turbulent viscosity is calculated by the Kolmogorov–Prandtl formula ($\mu_t = c_\mu\rho k^2/\varepsilon$).

The diffusion flows in the equations of the k–ε turbulence model are found from the relations

$$\alpha_i = \left(\mu + \frac{\mu_t}{\sigma_k}\right)\frac{\partial k}{\partial x_i}, \quad \beta_i = \left(\mu + \frac{\mu_t}{\sigma_\varepsilon}\right)\frac{\partial \varepsilon}{\partial x_i}.$$

To calculate the production term of turbulence, we use the relation written with account for the Kato–Launder correction:

$$P = \mu_t|S||\Omega|, \quad |S| = (2S_{ij}S_{ij})^{1/2}, \quad |\Omega| = (2\Omega_{ij}\Omega_{ij})^{1/2}.$$

The components of the deformation rate tensor and the rotation tensor are of the form

$$S_{ij} = \frac{1}{2}\left(\frac{\partial v_i}{\partial x_j} + \frac{\partial v_j}{\partial x_i}\right), \quad \Omega_{ij} = \frac{1}{2}\left(\frac{\partial v_i}{\partial x_j} - \frac{\partial v_j}{\partial x_i}\right),$$

The following values are assigned to the constants of the turbulence model: c_μ = 0.09, σ_k = 1.0, σ_ε = 1.3, $c_{\varepsilon 1}$ = 1.44, $c_{\varepsilon 2}$ = 1.92.

Numerical Realization. Calculations of the fluid flow field and the temperature field in the solid body are carried out one after another with subsequent load transfer between the two calculation regions. In simulating the conjugate heat transfer, the heat flow density is transferred from the fluid to the solid body and a temperature exchange between the fluid and the metal at the interface is assumed. In the case of noncoincidence of the finite-element and finite-volume meshes at the interface, interpolation of the boundary condition is used [12].

To discretize Eq. (1), the finite-element method [14] and the implicit time scheme [12] are used. To solve the system of difference equations, the Newton iteration method is used. To simplify its realization, in calculating the Jacobian, the derivatives of thermophysical parameters with respect to the temperature are neglected [14]. As the initial approximation of the solution, linear extrapolation of the temperature from the previous time step is used. Iterations terminate if the residual does not exceed the given accuracy (in the calculations 10^{-3}). To renew the solution, we use the method of lower relaxation with index 0.5. For preconditioning, the conjugate-gradient method is employed.

To discretize Eq. (2), we use the finite-volume method on the basis of a Runge–Kutta scheme of the 5th order with respect to time, a MUSCL scheme for discretizing nonviscous flows, and a second-order central scheme for discretizing viscous flows [15]. To solve the difference equations, a multimesh method (V-cycle and four levels of the mesh) is used.

The discretization of basic equations and boundary conditions is discussed in detail in [12, 15].

Time Step Control. The implicit scheme used to integrate Eq. (1) is undoubtedly stable. Therefore, the integration time step is chosen proceeding from the design accuracy of temperature calculation. To control the integration time step of Eq. (1), the accuracy parameter for the temperature ΔT was introduced (in the calculations ΔT = 1 K).

To vary the integration time step, we use an algorithm based on linear and parabolic time interpolation of the temperature. For each node of the finite-element mesh, the temperature at a current and two previous instants of time is determined. The three time points obtained are connected by straight lines and a parabola. The error is calculated at the point $\theta\Delta t$ (the parameter θ = 0.8 determines the type of the difference scheme) by the formula

$$\delta T = \frac{\theta \Delta t}{t_3 - t_1} \left| \frac{T_3 - T_2}{t_3 - t_2} - \frac{T_2 - T_1}{t_2 - t_1} \right| ,$$

where $\Delta t = t_3 - t_2$.

The temperature is determined on two sequential time layers with a step Δt_c (as the initial approximation, it is assumed that $\Delta t_c = 0.25 t_f$, where t_f is the finite instant of time). In the absence of reasons for restricting the integration time step the further calculation is carried out with a step Δt_o which is estimated proceeding from the convergence of the iteration process and the temperature calculation error.

The reasons for restricting the integration time step are the slow convergence of iterations (a slow decrease in the residual) and the nonfulfillment of the temperature accuracy condition on the time layer.

A new integration time step is chosen from the condition

$$\Delta t_o = \min \left\{ \Delta t_{o1}, \Delta t_{o2} \right\} .$$

For the time step not to be too small, it is fitted so that the remaining time interval holds an integral number of steps.

The time step Δt_{o1} depends on the temperature calculation error at the previous time step and the value of the temperature accuracy parameter given by the user:

$$\Delta t_{o1} = \Delta t^n \left(\frac{\Delta T}{\delta T} \right)^{1/2} .$$

Under the condition $\delta T > 2\Delta T$ (the obtained temperature change on the time layer is beyond the degree of accuracy of the temperature given by the user) the time step will decrease by one-half.

In choosing a new time step, we also take into account the possibility of its restriction because of the too slow speed of the iteration procedure called upon to match the temperature values of the metal and the fluid at the interface. The time step Δt_{o2} is obtained from the relation

$$\Delta t_{o2} = \frac{1}{4} \Delta t^n \left(\frac{N}{n} \right)^{1.3333} ,$$

where n is the number of iterations on a time layer; N is the maximum number of iterations on each time layer (in the calculations N = 20). The time step decreases by one-half when the maximum number of iterations is attained (at $n = N$).

Convergence Condition. Equations (1) and (2) are solved at boundary conditions of the 1st kind, and the surface temperature is determined from the equality of the heat flows and redetermined as a result of iterations.

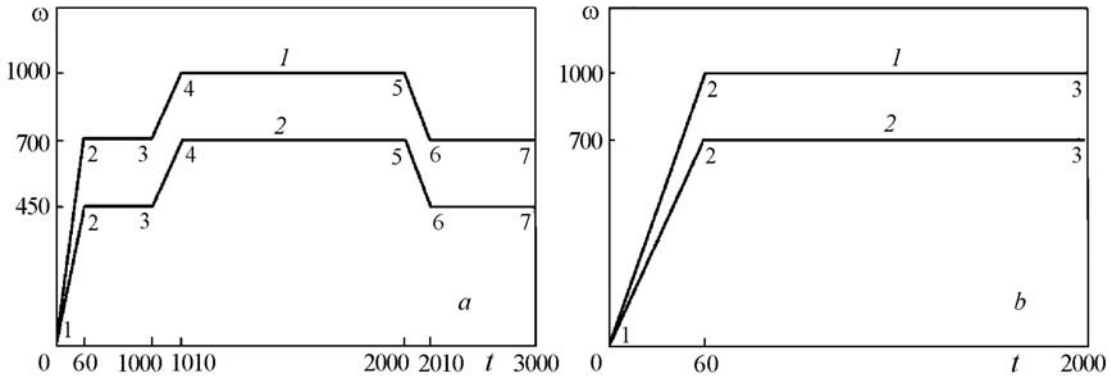

Fig. 3. Loading cycles for thermal modeling (a) and conjugate calculations (b). ω, 1/sec; t, sec.

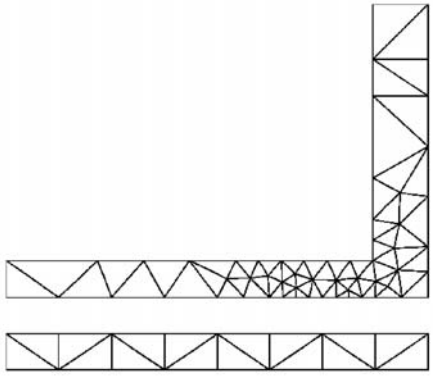

Fig. 4. Finite-element mesh in the two-dimensional case.

Matching of the values of the sought functions on the time step is provided by simple iterations. In so doing, the temperature-dependent values of the functions and the value of the interface temperature are redetermined. Iterations terminate when the mismatch between the metal and fluid temperatures at the interface turns out to be lower than the given value (in the calculations $0.25\Delta T$).

Loading Cycle. The loading cycles used for the two-dimensional and three-dimensional thermal simulation and conjugate calculations are shown in Fig. 3. Variable parameters are the angular rotational velocities of the disc (line 1) and the shaft (line 2).

In the case of thermal simulation, the length of the loading cycle is 3000 sec (Fig. 3a), including two portions of the rotation acceleration of the disc and the shaft (portions between points 1 and 2, 3 and 4), the rotation slowing-down portion (portion between points 5 and 6), and three portions characterized by a constant angular rotational velocity of the disc and the shaft (portions between points 2 and 3, 4 and 5, 6 and 7).

In the coupled thermal analysis, the rotor and the shaft, still at the initial instant of time, in 60 sec accelerated to a velocity of 1000 1/sec and 700 1/sec (portion between 1 and 2) respectively (Fig. 3b). The braking temperature in the inlet cross-section of region I decreases from 500 K at t = 0 to 450 K at t = 60 sec, and the braking temperature in the inlet cross-section of region II increases from 500 K at t = 0 to 700 K at t = 60 sec. A long time interval (t_f = 2000 sec) is used to let the metal temperature reach a steady-state value (portion between points 2 and 3). The use of a modified loading cycle in conjugate calculations is due to the necessity of reducing the processor time.

Computational Meshes. In the two-dimensional case, the finite-element mesh contains 87 triangular cells and 235 nodes (Fig. 4), and in the three-dimensional case 2170 cells and 4804 nodes.

The structured finite-difference mesh used in region I (Fig. 5a) contains 12,768 cells and 14,820 nodes (the inner surface of the rotor and the shaft surface hold 741 faces each, the inflow and outflow boundaries of the region contain 228 faces each). The structured finite-difference mesh used in region II (Fig. 5b) contains 303,471 cells and

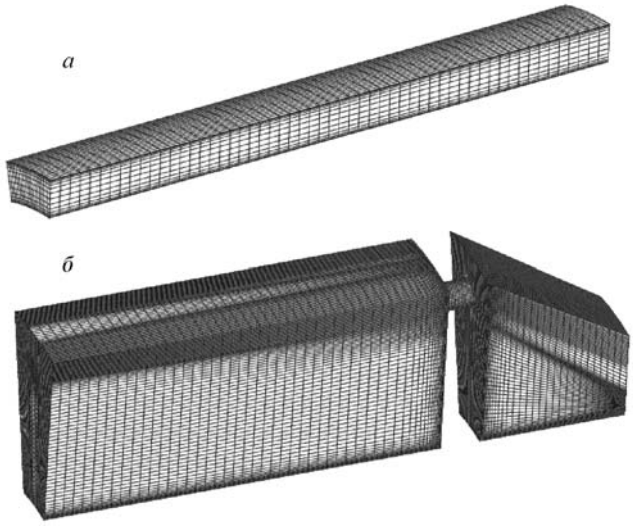

Fig. 5. Structured mesh in region I (a) and region II (b).

320,512 nodes (on the outer surface of the rotor there are 1862 faces, the left and right surfaces of the disc contain 3162 faces each, and the inflow and outflow boundaries of the regions contain 3591 faces each).

On all the surfaces that are of interest for coupled thermal analysis (the inner and outer surfaces of the rotor and the shaft surface) the coordinate y^+ varies over a range acceptable for the application of the wall function method ($35 < y^+ < 175$). On the left and right surfaces of the disc, the coordinate y^+ has a practically uniform distribution ($y^+ = 120$).

Boundary Conditions. At the initial instant of time $t = 0$ the metal has a uniform temperature distribution ($T_0 = 300$ K).

The formulation of the boundary conditions for the thermal simulation is explained by Fig. 1a. The thermal boundary conditions are identical in the two- and three-dimensional cases (in the two-dimensional case the boundary conditions are applied to edges, and in the three-dimensional one to faces).

At boundaries 1, 2, and 3, the fluid convection at a known temperature of the wall derived from the loading cycle for a given instant of time is taken into account. The heat transfer coefficient is calculated by means of the correlation dependence for a free rotating disc [16]. It is assumed that at $\mathrm{Re} < 2.4 \cdot 10^5$ laminar flow conditions are realized, and at $\mathrm{Re} > 3 \cdot 10^5$ turbulent conditions. In the interval between the above limiting values, linear interpolation is used. The correlation parameter is the angular rotational velocity of the disc.

In formulating the boundary conditions at boundaries 4 and 5, the formation mechanism of an adequate fluid flow in the rotating horizontal layer in the presence of a temperature gradient along the boundary is taken into account. The mass flow of the fluid into the annular gap between the disc and the shaft, the temperature, and the pressure are in compliance with the given loading cycle. The heat transfer coefficient is calculated by the correlation dependence for the forced convection of the fluid in the annular gas, whose parameters are the cross-section area, the hydraulic diameter, and the channel length.

At boundary 6, the heat transfer coefficient determined from the correlation dependence for the case of free-convective fluid flow on a vertical plate is given. A correlation argument is the plate length. As a wall temperature, the temperature obtained at boundary 10 is given.

The heat transfer coefficient at boundary 7 is calculated by the correlation dependence for a free rotating disc [16] (as at boundaries 1–3). The boundary temperature is obtained as a result of mixing of the flows along boundaries 4 and 5 and boundary 6 (the heat balance condition is used).

To formulate the boundary conditions on the inner surface of a hole (boundaries 8 and 9) and calculate the heat transfer coefficient, we use the correlation dependence for the forced convection of the fluid in the horizontal channel. Correlation arguments are the flow area, the hydraulic diameter, the channel length, and the flow rate of the fluid. The flow rate of the fluid (1/24 of the total rate of flow for the two-dimensional model), the temperature, and the pressure are derived from the loading cycle for a given instant of time.

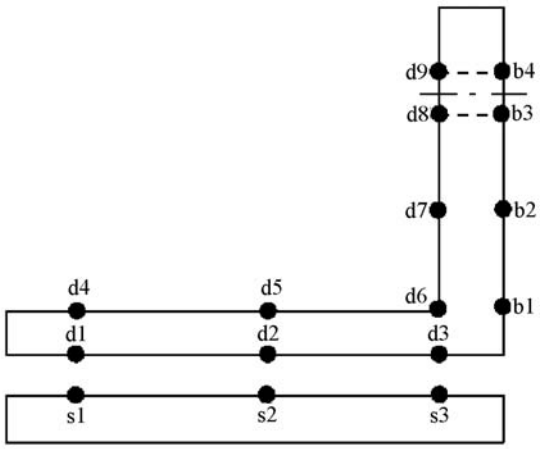

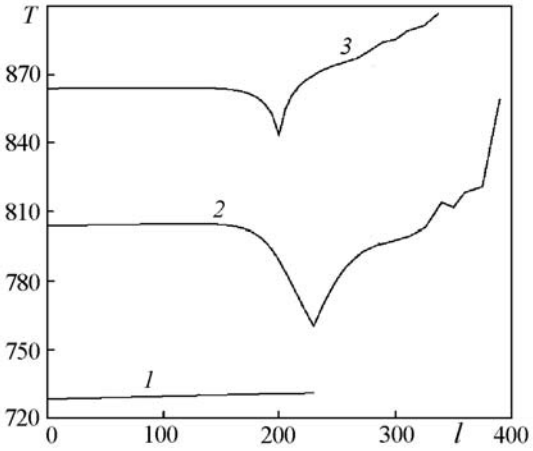

Fig. 6. Position of control points.

Fig. 7. Temperature distribution along the disc and shaft surfaces at time 2000 sec. T, K; l, mm.

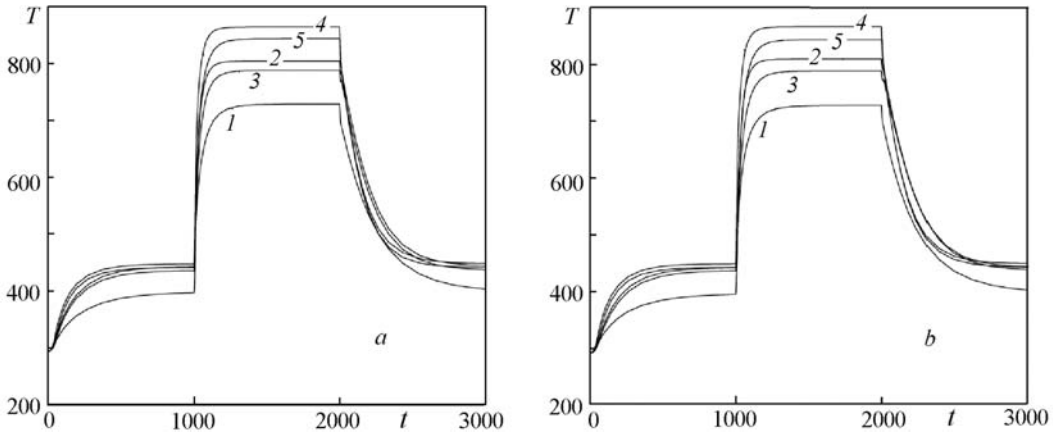

Fig. 8. Time dependence of the metal temperature at control points s1 (line 1), d1 (2), d3 (3), d4 (4), and d5 (5) in the two- (a) and three-dimensional (b) cases. Results of the thermal modeling. T, K; t, sec.

In formulating the boundary conditions at boundary 10, it is assumed that the fluid flowing past a given surface has a negligibly small heat capacity. The heat transfer coefficient is calculated by the correlation dependence for the free convection of the fluid in a horizontal cylinder. A correlation argument is the Grashof number calculated by the characteristic diameter and the rotational velocity.

In the coupled thermal analysis, on the inner and outer surfaces of the rotor, on the surface of the shaft, as well as on the left and right surfaces of the disc (boundaries 1, 4–9), conjugate boundary conditions are set. On the other walls of the model the boundary conditions remain unaltered.

For the velocity on the shaft and disc surfaces (in regions I and II) adhesion and no-flow boundary condition are set (Fig. 1). On the top and bottom surfaces of the blocks joined to the inlet cross-section of region I, as well as to the inlet and outlet cross-sections of region II, the sliding conditions are used. At the inflow boundaries, the mass flow (m = 0.63 kg/sec for region I and m = 2.25 kg/sec for region II) and the braking temperature (T = 500 K for region I and T = 700 K for region II) are given, and at the outflow boundaries a static pressure ($p = 5 \cdot 10^5$ Pa for region I and $p = 10^6$ for region II) is fixed. The flow direction is assumed to be normal to the inflow boundary. The turbulence characteristics at the inflow boundaries are assigned values of $k = 10^{-3}$ m^2/sec^2 and $\varepsilon = 10^{-2}$ m^2/sec^2. In the circular direction, periodic boundary conditions are used. In the data transfer from the three-dimensional CFD-model to the two-dimensional FEA-model, averaging of the flow parameters in the circular direction is performed.

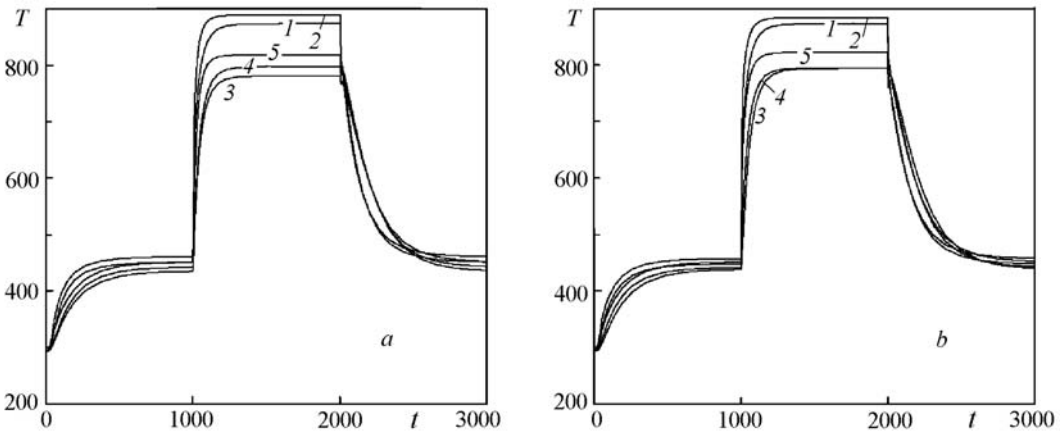

Fig. 9. Time dependence of the metal temperature at control points d7 (line 1), d8 (2), b1 (3), b2 (4) and b3 (5) in the two- (a) and three-dimensional (b) cases. Results of the thermal modeling. T, K; t, sec.

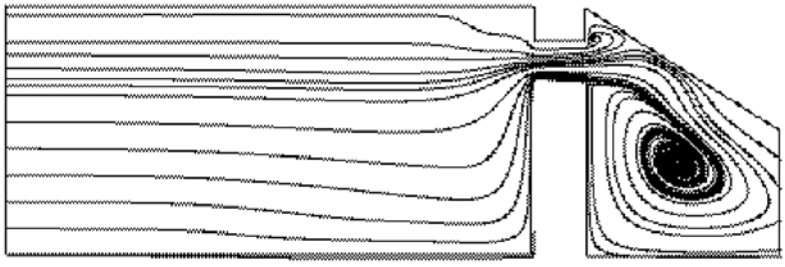

Fig. 10. Streamlines in the meridional section of region II.

The linear and rotational Reynolds numbers calculated by the parameters in the inlet cross-section and the angular rotational velocity of the disc are $8.89 \cdot 10^5$ and $1.51 \cdot 10^4$ for region I and $4.12 \cdot 10^4$ and $5.98 \cdot 10^4$ for region II, which corresponds to turbulent flow conditions.

Results of the Calculations. For the initial temperature field, the distribution obtained for the case of heat-insulated walls of the cavity is used. The position of control points on the disc and shaft surfaces at which the temperature is measured is shown in Fig. 6.

Thermal simulation. The temperature distributions along the outer surface of the shaft (line 1) and on the inner and outer surfaces of the disc (lines 2 and 3) are shown in Fig. 7. By l is meant the distance along the wall beginning with the left boundary of the calculation region. The kink of the curve corresponds to a nodal point of the modal. The temperature on the disc surface increases by about 100 K with increasing radial coordinate.

The time dependences of the metal temperature are shown in Fig. 8 and Fig. 9 (the results of calculations at points s1–s3, d1 and d2, d8 and d9, b3 and b4 practically coincide and, therefore, are not given in the figures). There is good agreement between the results obtained in the two- and three-dimensional formulations of the problem. The maximum difference between the metal temperatures at control points does not exceed 2 K (curves 3 and 4 in Fig. 9).

Coupled thermal analysis. The flow in a hole is practically symmetric. Weak asymmetry of the flow takes place only in the upper and lower regions. In the lower part of the cavity situated behind the hole, a recirculation zone occupying the entire volume of the working region is formed (Fig. 10). The secondary vortex is in the upper part of the cavity.

Except for the small initial portion that is due to the influence of the flow conditions at the inlet to the calculation region, the temperature distribution is practically uniform over the cross-section. This permits using the two-dimensional model for simulating conjugate heat transfer in region I.

In each time step, the number of iterations for calculating the fluid flow field in the cavity is assumed to be 100 for both models. The convergence condition is controlled by the temperature difference at the interface which equals 1 K.

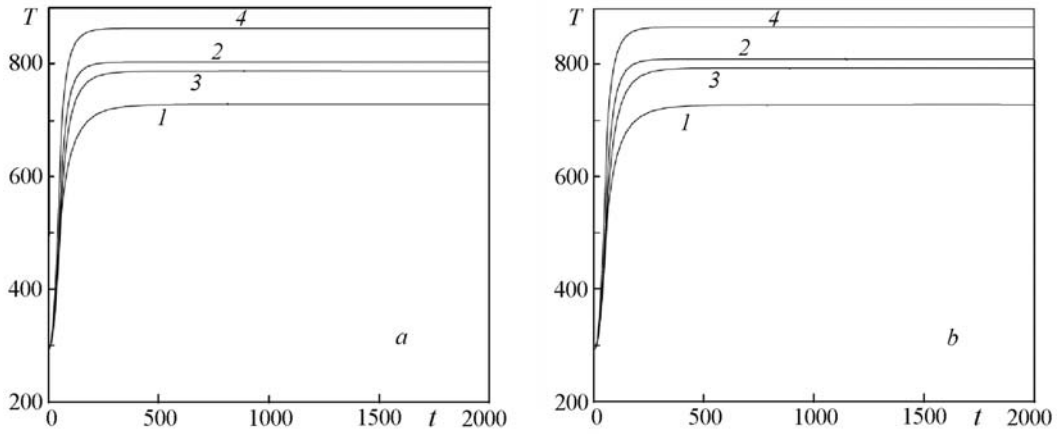

Fig. 11. Time dependence of the metal temperature at control points s1 (line 1), d1 (2), d3, (3), and d4 (4) in the two- (a) and three-dimensional (b) cases. Results of the coupled thermal analysis. T, K; t, sec.

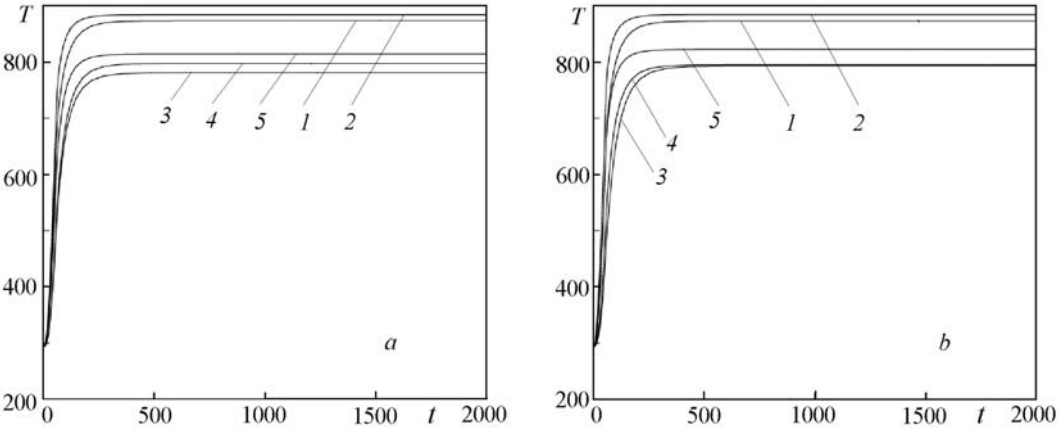

Fig. 12. Time dependences of the metal temperature at control points d7 (line 1), d8 (2), b1 (3), b2 (4), and b3 (5) in the two- (a) and three-dimensional (b) cases. Results of the coupled thermal analysis. T, K; t, sec.

The temperature distributions along the outer surface of the shaft and the inner and outer surfaces of the disc obtained in the conjugate formulation agree fairly well with the data presented in Fig. 7 obtained in using thermal boundary conditions based on the criteria relations for the heat transfer coefficient. However, the increase in the disc surface temperature given by the coupled thermal analysis is somewhat smaller and equals 90 K.

The time dependences of the metal temperature at control points obtained on the basis of the two- and three-dimensional coupled thermal analyses are given in Fig. 11 and Fig. 12 (the results of calculations at point s1–s3, d1 and d2, d4 and d5, d8 and d9, b3 and b4 practically coincide and, therefore, are not presented). There is fairly good agreement between the calculations in the two- and three-dimensional formulations. The greatest discrepancy between the calculation results are observed at points b1 and b2 (Fig. 12). The results of the computational modeling presented in Figs. 11 and 12 agree with the data obtained for the complete loading cycle and shown in Figs. 8 and 9 (for a time internal $1000 < t < 2000$ sec). The temperature calculation error corresponding to the steady-state conditions (horizontal portion of the loading cycle) does not exceed 1 K.

Conclusions. Computational modeling of the turbulent flow and conjugate heat transfer under the conditions of rotation of a disc with holes in an unbounded mass of a viscous compressible fluid has been carried out. The conjugate thermal calculations are based on the use of a nonstationary heat conduction equation describing the temperature distribution in a solid body and Reynold-averaged Navier–Stokes equations closed with the help of the k–ε-model of

turbulence for determining the velocity, pressure, and temperature distributions in the regions occupied by the fluid. Matching of the metal and fluid temperature at the interface is carried out by the iteration procedure.

To control and vary the integration time step, a temperature accuracy parameter that permits flexible control of the computational process was introduced.

Space-time temperature and thermal flow distributions at the metal-fluid interface in the two- and three-dimensional formulations of the problem have been obtained. The results of the computational modeling based on the formulation of the thermal boundary conditions by means of correlation dependences for the heat transfer coefficient and the results of the conjugate thermal modeling are in fairly good agreement with one another.

The results of the calculations are important for designing and optimizing components of gas turbines and compressors, as well as for subsequent modeling of their stressed-strained state and strength analysis under unstable or transient operating conditions.

NOTATION

a, shaft radius, m; *b*, disc radius, m; *c*, specific heat capacity of the metal, J/(kg·K); c_p, specific heat capacity of the gas at a constant pressure, J/(kg·K); c_μ, $c_{\varepsilon 1}$, $c_{\varepsilon 2}$, constants of the turbulence model; *d*, hole radius, m; *e*, total energy of a mass unit, J/kg; **F**, flow vector; **H**, source term; *k*, kinetic energy of turbulence, m^2/sec^2; *l*, length, m; *m*, specific mass flow, kg/sec; *n*, number of iterations; *N*, maximum number of iterations; *p*, pressure, Pa; *P*, production term of turbulence; Pr, Prandtl number; *q*, heat flow, W/m^2; **Q**, vector of conservative variables; *r*, radius, m; Re, Reynolds number; *s*, thickness, m; *S*, strain rate tensor; *t*, time, sec; *T*, temperature, K; v_x, v_y, v_z, velocity components, m/sec; *x*, *y*, *z*, Cartesian coordinates, m; α, β, diffusion flows in the equations of the turbulence model; γ, deviation of heat capacities; δ_{ij}, Kronecker symbol; ε, turbulent energy dissipation rate, m^2/sec^3; θ, parameter of the difference scheme; λ, heat conductivity, W/(m·K); μ, dynamic viscosity, kg/(m·sec); ρ, density, kg/m^3; σ_k, σ_ε, constants of the turbulence model; τ, shear stress, N/m; ω, angular rotational velocity, 1/sec; Ω, rotation tensor. Subscripts: c, current; e, effective; f, finite; *i*, *j*, tensor indices; *n*, time layer; o, optimal; t, turbulent; *x*, *y*, *z*, projections on the coordinate axes; w, wall; 0, parameters at the initial instant of time; +, dimensionless parameters in the boundary layer.

REFERENCES

1. D. Bohn, U. Kruger, and K. Kusterer, Conjugate heat transfer: an advanced computational method for the cooling design of modern gas turbine blades and vanes, in: *Heat Transfer in Gas Turbine*, WIT Press, Southampton (2001), pp. 58–108.
2. D. L. Rigby and J. Lepicovsky, Conjugate heat transfer analysis of internally cooled configurations, *ASME Paper*, No. 2001-GT-0405 (2001).
3. Y. Okita and S. Yamawaki, Conjugate heat transfer analysis of turbine rotor–stator systems, *ASME Paper*, No. 2002-GT-30615 (2002).
4. D. Bohn, J. Ren, and K. Kusterer, Conjugate heat transfer analysis for film cooling configurations with different hole geometries, *ASME Paper*, No. 2003-GT-38369 (2003).
5. K. Kusterer, D. Bohn, T. Sugimoto, and R. Tanaka, Conjugate calculations for a film-cooled blade under different operating conditions, *ASME Paper*, No. 2004-GT-53719 (2004).
6. L. V. Lewis and J. I. Provins, A non-coupled CFD–FE procedure to evaluate windage and heat transfer in rotor–stator cavities, *ASME Paper*, No. GT2004-53246 (2004).
7. K. Saunders, S. Alizadeh, L. V. Lewis, and J. Provins, The use of CFD to generate heat transfer boundary conditions for a rotor–stator cavity in a compressor drum thermal model, *ASME Paper*, No. GT2007-28333 (2007).
8. H. Li and A. J. Kassab, A Coupled FVM/BEM approach to conjugate heat transfer in turbine blades, *AIAA Paper*, No. 94-1981 (1994).
9. J. A. Verdicchio, J. W. Chew, and N. J. Hills, Coupled fluid/solid heat transfer computation for turbine discs, *ASME Paper*, No. 2001-GT-0123 (2001).
10. A. V. Mirzamoghadam and Z. Xiao, Flow and heat transfer in an industrial rotor-stator rim sealing cavity, *J. of Eng. for Gas Turbines and Power*, **124**, No. 1, 125–132 (2002).

11. J. Illingworth, N. Hills, and C. Barnes, 3D fluid-solid heat transfer coupling of an aero-engine preswirl system, *ASME Paper*, No. 2005-GT-68939 (2005).
12. K. N. Volkov, Solution of conjugate heat transfer problems and transfer of thermal loads between a fluid and a solid body, *Vych. Metody Programmir.*, **8**, No. 1, 265–274 (2007).
13. Z. Sun, J. W. Chew, N. J. Hills, K. N. Volkov, and C. J. Barnes, Efficient FEA/CFD thermal coupling for engineering applications, *ASME Paper*, No. GT2008-50638 (2008).
14. O. C. Zienkiewicz, *The Finite Element Method in Engineering Science*, McGraw-Hill, New York (1977).
15. K. N. Volkov, Use of the control volume method for solving problems of the fluid and gas mechanics of on nonstructured grids, *Vych. Metody Programmir.*, **6**, No. 1, 43–60 (2005).
16. A. Northrop and J. W. Owen, Heat transfer measurements in rotating disc systems — the free disc, *Int. J. Heat Fluid Flow*, **9**, No. 1, 19–26 (1988).